The Journal of The Textile Institute
2023, Volume 114, Issue 7, Pages 998-1006
https://doi.org/10.1080/00405000.2022.2105075
https://archimer.ifremer.fr/doc/00789/90132/

Experimental evaluation of the main parameters influencing friction between polyamide fibers and influence of friction on the abrasion resistance

Bain Cédric [1, 2, 3, *], Davies Peter [1], Riou Luc [1], Marco Yann [2], Bles Guilhem [2], Damblans Guillaume [3]

[1] IFREMER, Centre Bretagne, Plouzané, France
[2] ENSTA Bretagne, Institut de Recherche Dupuy de Lôme IRDL-UMR CNRS 6027, Brest, France
[3] France Energies Marines, Brest, France

* Corresponding author : Cédric Bain, email address : cedric.bain@ensta-bretagne.org

Abstract :

Friction is one of the key factors in the manufacture of ropes, and has an important influence on the mechanical behavior of many fiber assemblies. For this reason, the understanding and the evaluation of the coefficients of friction between fibers is an essential step in the development of numerical rope models. This paper describes tests on a modified, upscaled version of the ASTM (American Society for Testing and Materials) standard yarn-on-yarn abrasion test device, which allows measurement of the friction coefficient between polyamide rope yarns. It is shown that the inter-fiber angle has a significant influence on the friction coefficient, and the direction of movement relative to the filament has to be considered in the determination of this coefficient. A normalized representation allows friction coefficients measured for a range of test conditions to be plotted on a single curve. The abrasion test device allows the friction coefficient to be measured throughout abrasion tests. It is concluded that lower friction leads to higher abrasion resistance and longer lifetime.

Keywords : : Friction, polyamide, fibers, abrasion, lay length

Introduction

Synthetic fiber ropes are widely used in mooring lines thanks to their numerous qualities: light weight, good mechanical properties and excellent marine resistance. The mechanical property /linear density ratio is more interesting for synthetic ropes than for the steel cables which are currently used. Chevillotte et al. (2020); Ridge et al. (2010) and Weller et al. (2015) have shown the attractivity of polyamide ropes for mooring lines: low cost and modulus, higher elongation than the polyester fibers mostly used for moorings offshore today, and equivalent ultimate tensile strength. Polyamide appears particularly well-suited for floating offshore wind turbine moorings, (Ridge et al., 2010). To understand more specifically the mechanisms that occur in a mooring line, meso-scale models can be developed (Davies et al., 2016; Durville, 2010; Vu et al., 2015). These allow material properties and construction parameters to be examined. The friction between rope elements is one of the key input parameters for these models, as it affects the internal movements of fibrous assemblies and hence the mechanical behavior (Cornelissen et al., 2013). Several previous studies (Gassara et al., 2018; Leech, 2002) have noted that there are various fiber/fiber friction interactions, depending on their orientations, such as: longitudinal-to-longitudinal, longitudinal-to-transverse, transverse-to-transverse. Under mechanical load, fibers reorient (Bain et al., 2020), which changes the angles between the fibrous elements, and so this will also affect friction values (Leech, 2002; Lindberg & Gralén, 1948). In order to quantify this effect, published work has focused on the influence of the main parameters; the angle between fibers, and the tension in them. For example, two recent studies have been performed on carbon fibers using a capstan type experimental device (Chakladar et al., 2014; Tourlonias et al., 2019).

In the present study an experimental device based on a modified, upscaled version of the ATSM (American Society for Testing and Materials) standard yarn-on-yarn test was used. This test, developed and analyzed previously (Flory et al., 1988; Goksoy, 1986; Hobbs & Ridge, 2018) is widely used in the rope industry to check the coatings on yarns. By adding load cells to measure the applied loads it was possible to determine friction coefficients for different configurations. The aim is to identify the main parameters which affect the friction behavior and to propose a friction law with as few parameters as possible. This will simplify the development of a meso-scale rope model. Also, with the same experimental device, abrasion tests were performed and enabled direct study of the relationship between the friction coefficient, the abrasion resistance and the cycles to failure. This result is directly linked to the durability of offshore mooring lines and the understanding of fiber assemblies.

1. Material and Methods

a. Material

The material used for this study is a polyamide 6 rope yarn with a specific coating provided by the rope manufacturer Bexco (Hamme, Belgium). It is a grade widely used for marine applications. As known from the literature, fibers in ropes are assembled at different scales. To be precise in the following study, Figure 1 shows the different scales of a sub-rope. Mooring lines for floating offshore platforms are generally made in a so-called "parallel sub-rope" construction, in which a number of sub-ropes (either twisted 3 or 4-strand or braided) are placed in parallel and held together by an outer braided cover; the number of sub-ropes is adjusted to meet the required specification. The different components of the sub-rope are the strand, the rope yarn, the yarn and the filament. The model sub-rope studied here is made of 3 strands, each strand is composed of 10 rope yarns, each rope yarn is composed of 13 yarns in a S-twist configuration and each yarn is made of several hundreds of filaments. The tested scale for this study is the ropeyarn, as friction results for this scale are needed for the development of the numerical meso-scale model.

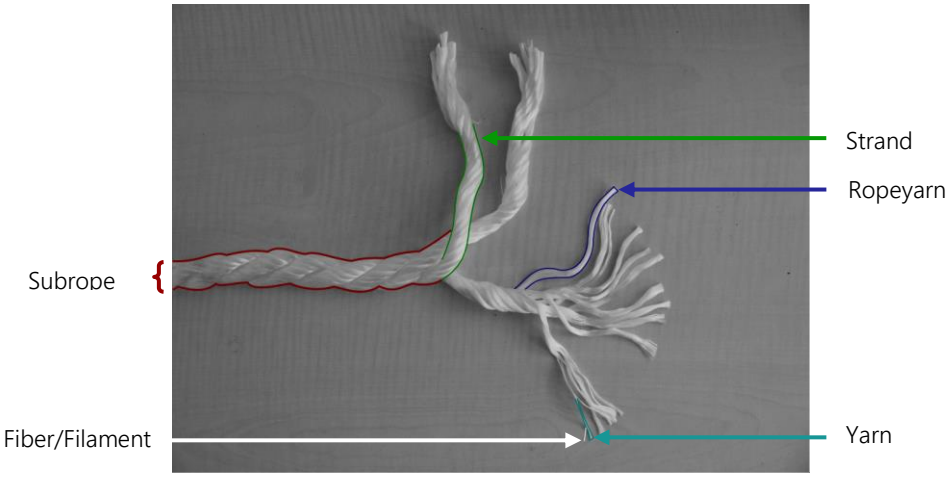

Figure 1. The different scales of a model 3-strand sub-rope

b. Experimental device

The experimental device used is based on the ASTM D3412-07 test standard for yarns but upscaled to test rope yarns. Figure 2 shows the experimental set-up used. It is similar to the experimental set-up used for yarn-on-yarn testing, but allows higher loads (up to 12.5 kg) and has larger diameter pulleys (50mm). One end of the rope yarns is fixed around a first pulley which is mounted on a rotating arm (on the right of the photo) which turns at a fixed frequency of $f_{rot} = 1\ Hz$. The rope yarn then passes over a 2nd, 3rd, 4th, 5th and 6th pulley and the other end is tied to a weight to apply a constant tension. Between the 3rd and 5th pulleys the yarn is twisted on itself. The twisted zone is immersed in a container filled with natural sea water.

Two load cells are placed between the 2nd and 3rd, and 5th and 6th pulleys, in order to measure the difference in force before and after the twisted friction zone. Output signals from these load cells are recorded with an HBM data logger.

The samples are taken from a coil of the studied ropeyarn. Their length is around 3 meters. The number of rotations in the twisted section for the study is $n = 3$.

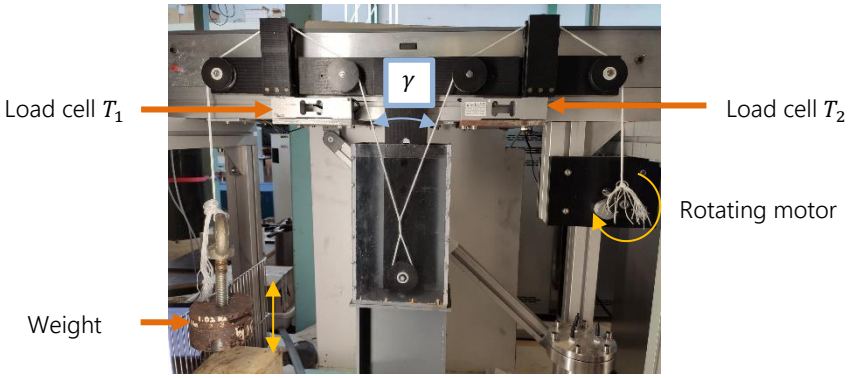

Figure 2. Experimental set up

c. Definitions and protocols

There is an analytical expression for the friction coefficient in the ASTM standard, which is based on the analysis of Goksoy (1986). However, Hobbs & Ridge (2018) identified an error in the expression and proposed an alternative analysis with fewer approximations. They found significantly greater values of the friction coefficient. The difference between the analysis of Goksoy (ASTM) and this more recent analysis are presented in figure 3.

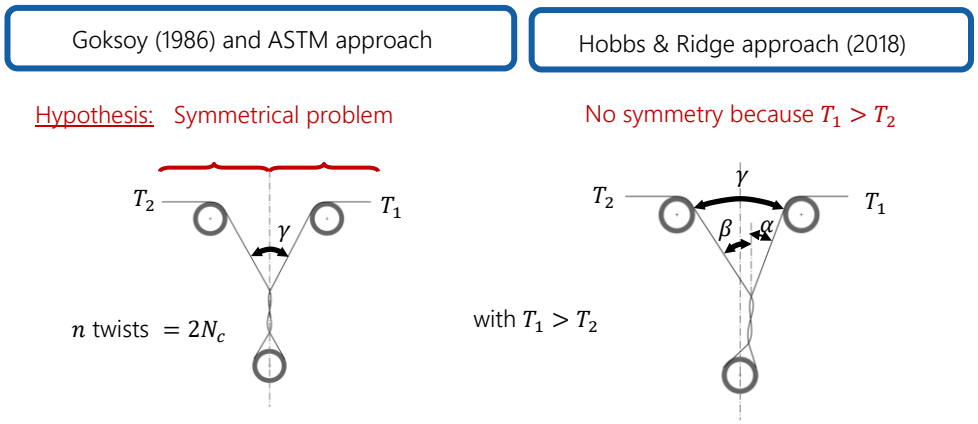

Figure 3. Differences between the Goksoy approach and Hobbs & Ridge approach

For Goksoy's analysis, the friction coefficient μ is given by:

$$\mu = \frac{\ln\left({}^{T_1}/_{T_2}\right)\tan\left({}^{\gamma}/_{2}\right)}{2\pi(N_c - 1)\sin^2\left({}^{\gamma}/_{2}\right)} \quad (1)$$

With n number of twists = $2N_c$

In the ASTM standard, this expression is simplified for small γ:

$$\mu = \ln\left(\frac{T_1}{T_2}\right)\frac{1}{2\pi n\gamma} \quad (2)$$

Hobbs and Ridge removed the hypothesis of a symmetrical problem, the friction coefficient μ is then given by:

$$\mu = \frac{(T_1 - T_2)\tan\left({}^{\gamma}/_{2}\right)}{\pi(N_c - 1)(T_1\sin^2\alpha + T_2\sin^2\beta)} \quad (3)$$

On Figure 4, the asymmetry can be clearly identified. For the present study, Hobbs' expression has therefore been used. The experimental set-up also requires a digital camera and LED lighting, in order to record the changes to angles α and β.

Figure 4. Image from the camera to identify the angles α and β

Due to the difficulty to detect markers through automatic software and programs, the angles α and β have been determined visually and with the software *Inkscape*. The angles were measured at a determined point in the cycle, which is the configuration when the weight is at the highest position. This simplifies the detection of the corresponding forces T_1 and T_2.

In a preliminary study the conclusion of Hobbs was confirmed; taking the asymmetry into account results in significantly higher friction values than those calculated using the standard test method, see Figure 5. For the remainder of this study the expression used to calculate the friction coefficient is equation (3).

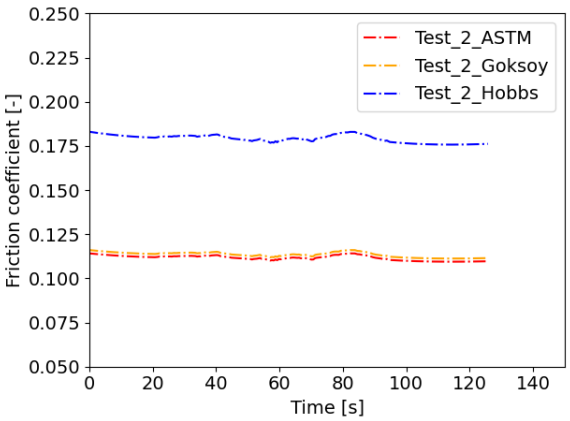

Figure 5. Example showing difference between the friction coefficient values calculated with the different approaches (mean curve of 3 tests is plotted).

The influence of two main parameters on the friction coefficient has been investigated:

- Tension
- Angle γ

The test time was fixed to around 100s which is equivalent to 100 cycles. Furthermore, to determine the friction coefficient a specific time of 80s of testing was arbitrarily chosen, in order to allow the geometry of the twisted area to stabilize.

Three different weights were used to vary the rope yarn tension. These were 2.74kg, 7.36kg and 12.38kg which correspond to 0.7%, 1.85% and 3.1% of the ropeyarn MBL (Mean breaking load). With the current experimental set-up, it was not possible to reach higher tension. To change the angle γ, several positions of the lowest pulley were examined, Figure 6. The position 3 corresponds to the standard pulley position according to the ASTM standard.

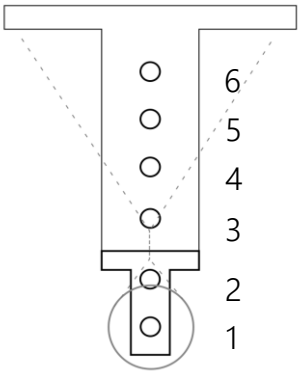

Figure 6. The different positions of the lowest pulley

With these different positions, the angle γ changes between 27° and 60°. For the study to investigate the influence of the tension, the lowest pulley was at the position 3.

2. Results and discussion

a. Influence of the tension and the angle γ

Figure 7.a. shows how the friction coefficient varies with the tension, while Figure 7.b. shows how it changes with the angle γ. On these two figures, each point represents the mean value from 3 tests.

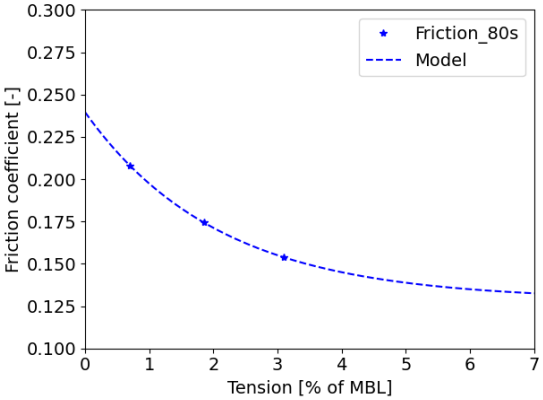

Figure 7.a. Variation of the friction coefficient with the tension

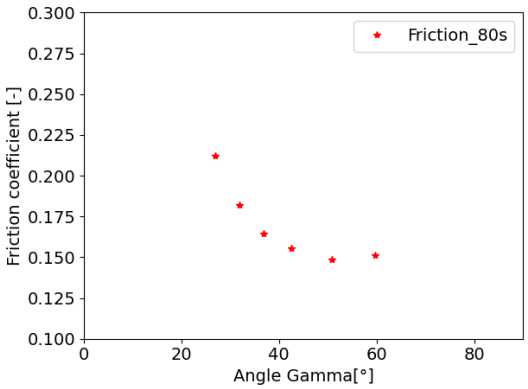

Figure 7.b Variation of the friction coefficient with the angle γ.

When the angle γ is changed the friction coefficient μ shows a significant drop before reaching a plateau.

In the literature there are few data for friction coefficients on polyamide fibers. Gassara et al. (2018) published a recent study on the friction coefficient of polyamide at the filament scale. That was the first

study to determine the longitudinal-longitudinal friction coefficient μ_{ll} and the transverse-transverse friction coefficient μ_{tt} (cf. Figure 8.a. and Figure 8.b.) simultaneously.

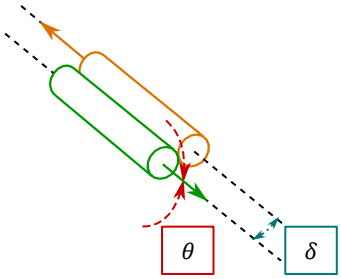

Figure 8.a. Longitudinal-longitudinal friction coefficient μ_{ll}

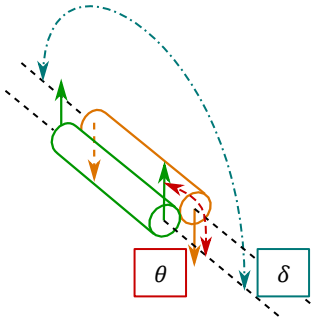

Figure 8.b. Transverse-transverse friction coefficient μ_{tt}

The data obtained by Gassara et al. (2018) indicate $\mu_{ll} \approx 0.25$ and $\mu_{tt} \approx 0.17$. The results shown here, for rope yarn on rope yarn friction, are in accordance with the literature. For low γ angle, the type of friction seems to be closer to a longitudinal-longitudinal friction coefficient, while for higher γ angle, it is closer to a transverse-transverse friction coefficient. This will be discussed further below, with the analysis of the inter-fibers angle δ and the friction angle θ.

The change in friction coefficient with the ropeyarn tension (Figure 7.a.) can be extrapolated by a fitting model described by the equation (4).

$$\mu(T) = ae^{-bT} + c \tag{4}$$

With T the tension of the ropeyarn, a, b and c constants determined by linear regression. However, according to the study of Gassara et al. (2018), the friction coefficient μ does not depend on the tension at the filament scale. On closer examination, the changes in μ with both the angle γ and the tension T are similar. This suggests a possible explanation for this observation: in the literature, it is well known that there is a rearrangement of fibers during a tension loading. Bain et al. (2020) observed this phenomenon on fibers assembled in braided ropes. This assumption was also made by Liu et al. (2006) to explain the evolution of the coefficient of friction with the yarn axial tension. It might therefore be assumed that the effect of applied tension is primarily an influence on the rearrangement of the filaments inside the rope yarns, and that it is this which governs the changes in μ.

To confirm this hypothesis, a second experimental campaign was performed, with measuring equipment added to characterize the filament geometry inside the ropeyarn.

b. Influence of the angle between filaments

In order to quantify the fiber angles a CANON EOS 100D digital camera with 18 million pixels was used with a standard lens with a focal length between 18mm and 55mm. Two pictures were taken before and after testing for both sides of the twisted area, cf Figure 9. To measure the helix angle φ of the filaments inside the ropeyarn, six measurements were made on each image. For each time step, two helix angles were obtained: left helix angle φ_l and right helix angle φ_r. For this study, the variation between these two angles was negligible, so $\varphi = \varphi_l = \varphi_r$.

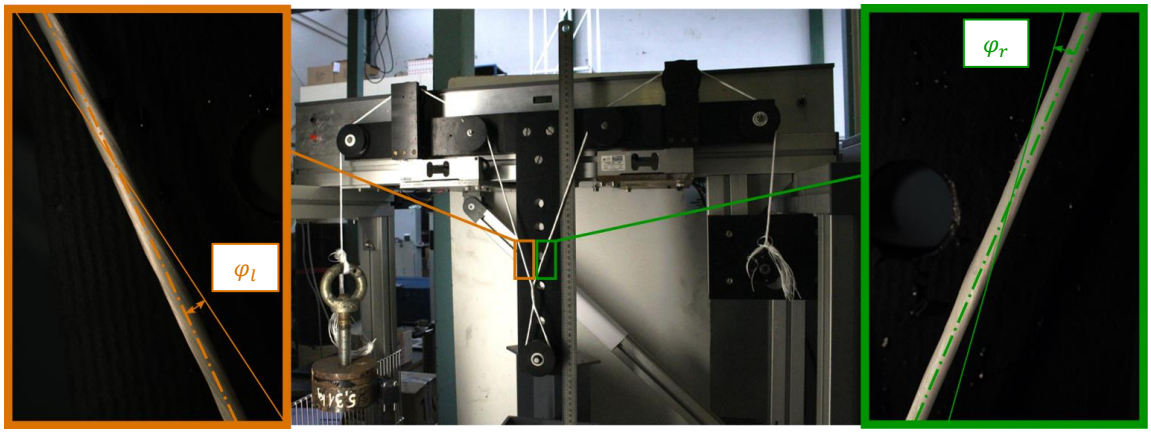

Figure 9. Raw data from camera to measure the helix angle φ

After several measurements throughout the experimental campaign, Figure 10 shows a fairly wide variation of the helix angle. The standard deviation before and after testing tends to decrease over time. For the remainder of the study, the helix angle after testing is considered as the stabilized helix angle.

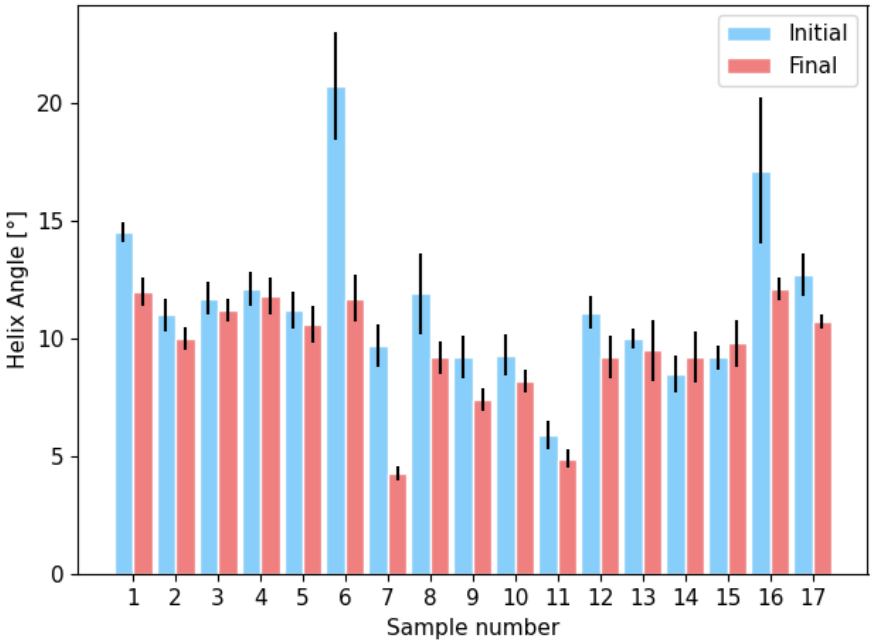

Figure 10. Evolution of the helix angle before and after testing

Once the helix angle was determined, the aim of the study was to determine the contact angle between the filaments of the rope yarns in the wrapped zone. In the remainder of the paper, this will be called the inter-fiber angle δ.

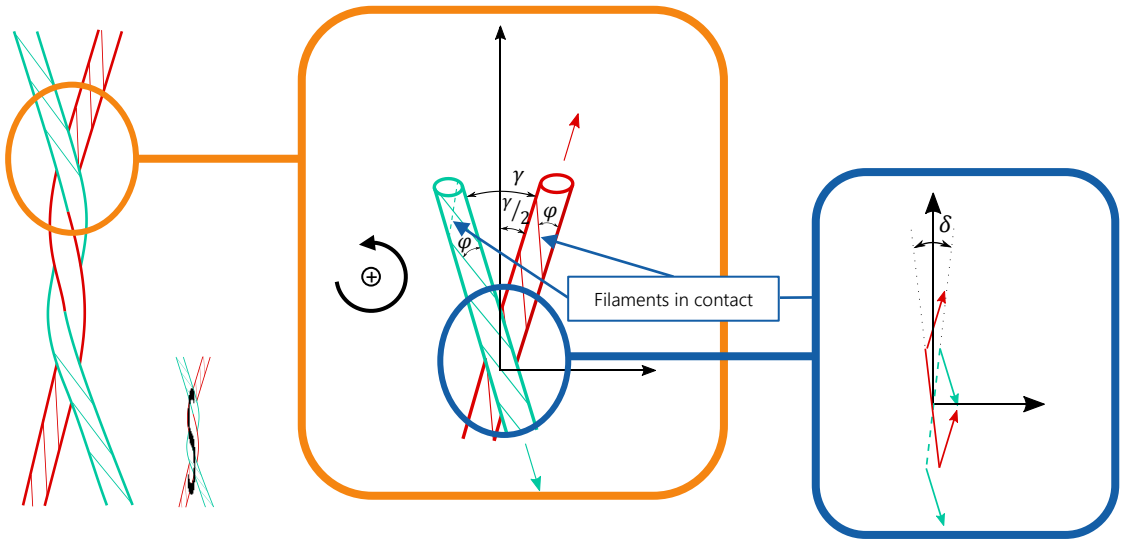

Figure 11. S-wrapped area for S-twisted rope yarn

There are two ways to twist fibers in a rope yarn: S twist (for left-handed twist) and Z-twist for right-handed). In this study all the rope yarns had S-twist. There are then two ways to install the ropeyarn sample in the test machine, as the twist zone can be wrapped using either S-wrapped (see Figure 11) or Z-wrapped (for

right-handed twist see Figure 12). Figure 11 shows the twisted area for S-wrapped rope yarn. The green ropeyarn corresponds to the left side of the experimental set-up. Its end is fixed to the weight. The red one corresponds to the right side of the experimental set-up. Its end is fixed to the rotating arm. The angle between these two rope yarns is characterized, as noted earlier, by the angle γ. Filaments inside each rope yarn are represented as the helix angle φ. The dotted green filament in the window on the right represents the filament in contact with the red ropeyarn. If anti-clockwise angles are defined as positive, the inter-fiber contact angle δ can be determined by the following expression:

$$\delta_S = \gamma - 2\varphi \tag{5}$$

For Z-wrapped rope yarn, the contact between the filaments from the green and the red rope yarns changes, Figure 12, as does the expression of the inter-fiber angle δ.

The expression of δ for Z-wrapped rope yarn is then:

$$\delta_Z = \gamma + 2\varphi \tag{6}$$

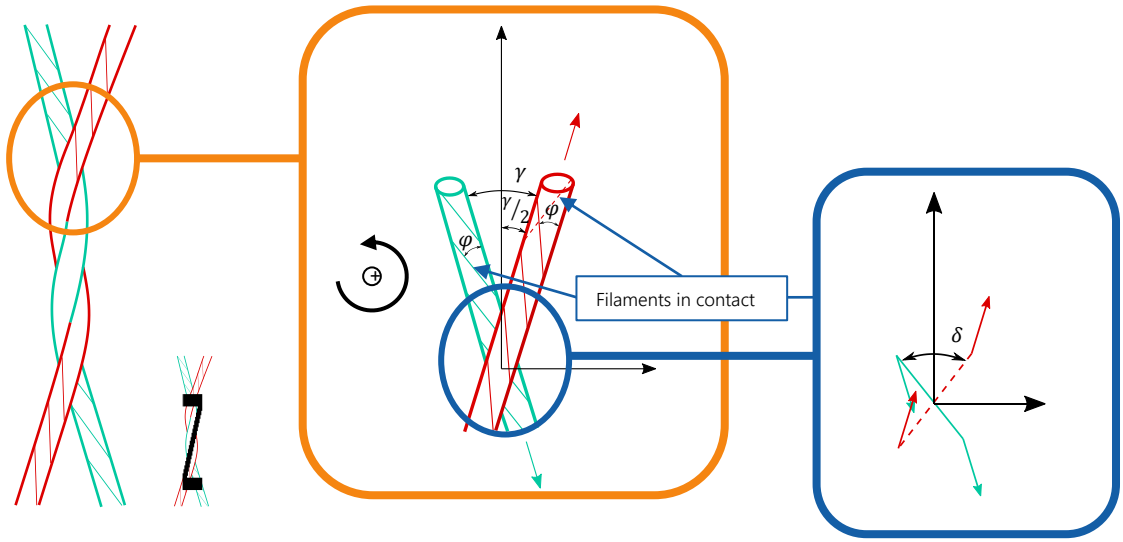

Figure 12. Z-wrapped area for S-twisted rope yarn

The aim of the experimental campaign is to quantify the changes in the friction coefficient with the inter-fiber angle δ. In order to have the widest possible range of angle δ for S-wrapped rope yarns, samples were unstranded by manually removing the twist from rope yarns (helix angle $\varphi = 0°$). Then S-wrapped rope yarns were tested for every pulley position for S-wrapped rope yarns and at pulley positions 4, 5, and 6 for S wrapped unstranded rope yarns. Also, Z-wrapped samples were tested for stranded and unstranded rope yarns at pulley position 3. The tension for all these samples was arbitrarily chosen to be 7.36 kg.

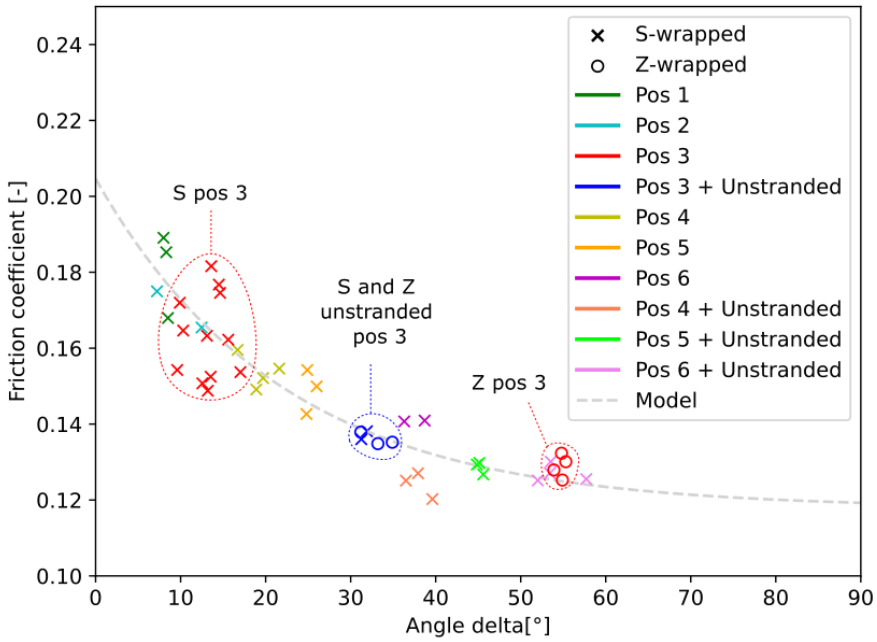

Figure 13. Evolution of the friction coefficient μ with the inter-fiber angle δ, S and Z wraps

Figure 13 shows the how the friction coefficient μ varies with the inter-fiber angle. It appears that the coefficient of friction μ decreases with increasing inter-fiber angle δ. The decrease is faster for low angles and tends to stabilize to a specific value at higher angles. The shape of this curve can be modeled by the same type of equation as (4). A similar change in the friction coefficient was found by Tourlonias et al. (2019), and Chakladar et al. (2014) on a similar scale for carbon fibers. For $\delta = 0°$, the angle between the filaments of the rope yarn correspond to the case of longitudinal-longitudinal friction. For this condition for the material of this study, we found $\mu_{ll} \approx 0.20$ which is reasonably close to the value obtained by (Gassara et al., 2018) for polyamide filaments ($\mu_{ll} \approx 0.25$). The lower value here can be explained by the use of a different coating and the fact that the tests here were performed in water. For $\delta = 90°$, the friction coefficient is around 0.12 but this is not the same as a transverse-transverse friction. The scatter of the experimental data can be explained by the variation of the helix angle φ along the ropeyarn. Some improvements may be possible in the determination of this angle. As Chakladar et al. (2014) concluded on carbon fiber tows, the inter-fiber angle is the main influence on the friction coefficient. The increase of friction coefficient for lower inter-fiber angle δ can be explained by the fact that the entanglement of fibers is easier than for high inter-fiber angle δ. Tourlonias et al. (2019) developed an analytical model to consider this interpenetration of the fibers between carbon tows.

Another important observation that can be made is the difference between the friction coefficient of S-wrapped and Z-wrapped ropeyarn zones for the same pulley position (see the two set of points outlined in red). Furthermore, samples with unstranded rope yarns were tested in S-wrapped and Z-wrapped

assemblies (see the set of points outlined in blue). The helix angles φ for these samples are around zero, so the inter-fiber angle δ is the same for both wraps and the friction coefficient would be expected to be the same. Indeed, experimentally, the friction coefficient is found to be the same and its value is equal to 0.14.

A closer look at the two configurations in Figure 8 indicates that for both kinds of friction the inter-fiber angle δ seems to be equal to 0°, so this angle alone is insufficient to characterize the fiber interactions. To account for this fact, the direction of movement relative to the filament has also to be considered. For this experimental set-up, it can be determined by the friction angle $\theta = \frac{\delta}{2}$. Indeed, by taking one filament as a reference, the relative movement between the two filaments is described by the friction angle β. Then for a longitudinal-longitudinal friction, $\theta = 0°$ and $\delta = 0°$. And for a transverse-transverse friction, $\theta = 90°$ and $\delta = 180°$. The Figure 14 represents the variation of the friction coefficient with the friction angle θ.

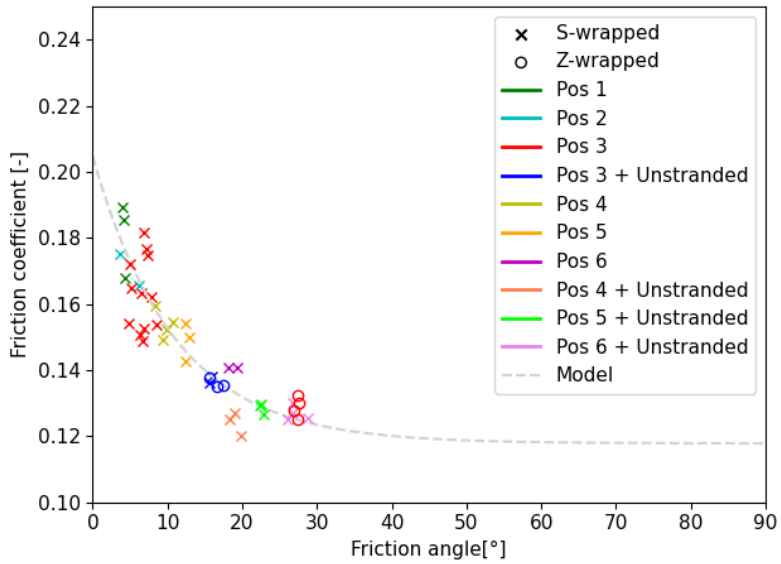

Figure 14. Evolution of the friction coefficient μ with the friction angle θ

With this representation on Figure 14, the transverse-transverse friction corresponding to a friction angle $\theta = 90°$ is estimated to be around 0.12. As for μ_{ll}, this value is close to the value obtained by Gassara et al. (2018).

This range of friction coefficients is not negligible, and friction has a strong influence on the mechanical behavior of fiber assemblies and their durability. A third experimental campaign was therefore performed to examine the influence of the friction coefficient on the abrasion durability.

c. Influence of the friction coefficient on the abrasion durability

In order to examine how friction coefficient affects lifetime under abrasive conditions a series of tests to failure were performed using the same rope yarn-on-rope yarn experimental set-up. Abrasion tests to failure were carried out in natural seawater at pulley position 3, on the same rope yarns which had been wrapped either in the S or Z direction in the twist zone. A load of 7.36 kg was applied and the weight was blocked in the horizontal plane during cycling, to stop it rotating and unwinding the ropeyarn.

The cycles to failure are given in Table 1. There is a very large difference between S and Z configurations, a factor of around 5 in lifetime, with the Z configuration surviving much longer than the S.

Samples number	Number of cycles to failure for S wrap	Number of cycles to failure for Z wrap
1	31531	141260
2	35333	162500
3	33717	162577
4	26583	154412
5	33530	152066
Mean	32139	154463

Table 1. Number of cycles to failure for abrasion tests with rope yarns twisted together and assembled in S and Z configurations.

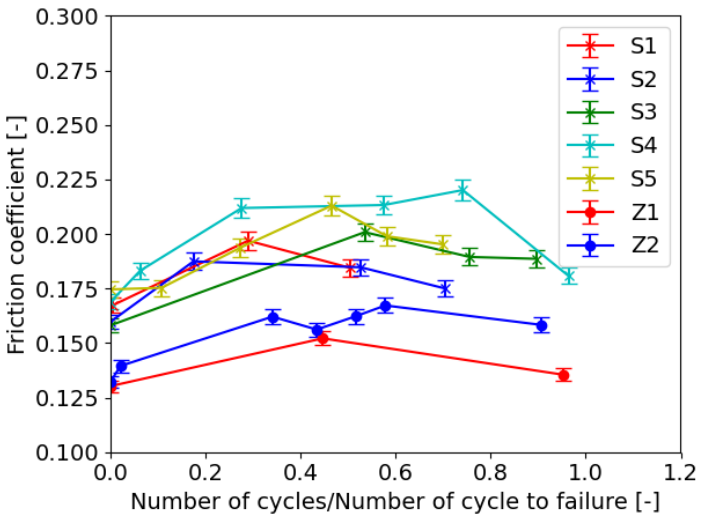

Figure 15. Evolution of the friction coefficient during abrasion test. Comparison between measurements made during tests, based on number of cycles normalized by cycles to failure, five S and two Z samples.

During the abrasion tests different friction measurements have been performed, Figure 15, and this provides a clear indication of the reason for the large difference in lifetimes. The friction coefficients for Z wrap are significantly lower than those for S wrap, not just initially, as noted previously, but throughout the tests. The data reveal that the initial friction coefficients are similar to those presented previously in Figure 14. Friction coefficients tend to increase initially during the tests in all cases, presumably as the coating is removed from the fibers, but then drops probably as damage to fibers starts to occur. An example of the damage in an S-wrapped sample S1 is shown in Figure 16.

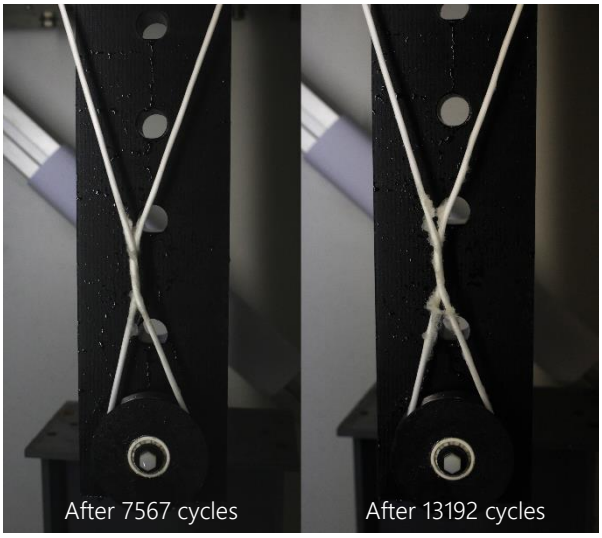

Figure 16. Damage during abrasion test of sample S1

In future standards it will be important to set the specific wrap (S or Z wrap) and twist to use (S or Z twist). These results also show that the friction coefficient μ is one of the main parameters controlling abrasion durability.

From a scientific point of view, it would also be interesting to generate more plots such as the one in Figure 15. A better understanding of the mechanisms corresponding to the changes in friction coefficient with cycling could provide the basis for future predictive durability modelling of ropes.

Conclusion

Variation of the friction coefficient between polyamide fibers in rope yarns was investigated through an experimental set-up based on the ASTM yarn-on-yarn standard test for the characterization of abrasion durability. The inter-fibers angle δ and the friction angle θ have been determined as the most important parameters controlling the friction coefficient for polyamide fibers. For increasing inter-fiber angle δ, the friction coefficient greatly decreases before reaching a plateau. All data from a wide range of test conditions fall on a single curve when friction coefficient is plotted versus inter-fiber-angle. This is a very useful result, which will be important in the development of a meso-scale numerical rope model.

To the authors' knowledge this is the first time that an instrumented abrasion experimental set-up has been applied to characterize the influence of the different angles on friction between rope yarns. The results obtained on the friction coefficient are in accordance with the literature from other experimental devices. The test also allowed the influence of these angles on the abrasion resistance of the fibers to be investigated. This revealed that the friction coefficient has a significant effect on the abrasion lifetime. Concerning test procedures, for abrasion tests on rope yarns the direction of wrap and the direction of twist used to assemble the yarns has to be specified, due to its strong influence on results.

The similar evolution of friction coefficients with inter-fiber angle between carbon fibers and polyamide fibers suggests it may be possible to extend these friction laws for other materials. Further investigations on different fibers and at different scales are underway.

Acknowledgements

The authors would like to thank all the partners of the MONAMOOR project and the French ANR Agency for their financial support.

Declaration of interests

☒ The authors declare that they have no known competing financial interests or personal relationships that could have appeared to influence the work reported in this paper.

☐ The authors declare the following financial interests/personal relationships which may be considered as potential competing interests:

References

Bain, C., Davies, P., Bles, G., Marco, Y., & Barnet, J. (2020). Influence of bedding-in on the tensile performance of HMPE fiber ropes. *Ocean Engineering*, *203*. https://doi.org/10.1016/j.oceaneng.2020.107144

Chakladar, N. D., Mandal, P., & Potluri, P. (2014). Effects of inter-tow angle and tow size on carbon fibre friction. *Composites Part A: Applied Science and Manufacturing*, *65*, 115–124. https://doi.org/10.1016/j.compositesa.2014.06.002

Chevillotte, Y., Marco, Y., Bles, G., Devos, K., Keryer, M., Arhant, M., & Davies, P. (2020). Fatigue of improved polyamide mooring ropes for floating wind turbines. *Ocean Engineering*, *199* (September 2019). https://doi.org/10.1016/j.oceaneng.2020.107011

Cornelissen, B., Rietman, B., & Akkerman, R. (2013). Frictional behaviour of high performance fibrous tows: Friction experiments. *Composites Part A: Applied Science and Manufacturing*, *44*(1), 95–104. https://doi.org/10.1016/j.compositesa.2012.08.024

Davies, P., Durville, D., & Do, T. (2016). The influence of torsion on braided rope performance , modelling and tests. *Applied Ocean Research*. https://doi.org/10.1016/j.apor.2016.07.003

Durville, D. (2010). *Simulation of the mechanical behaviour of woven fabrics at the scale of fibers*. *3*, 1241–1251. https://doi.org/10.1007/s12289-009-0674-7

Flory, J. F., Goksoy, M., & Hearle, J. W. S. (1988). Yam-on-yarn abrasion testing of rope yarns part i: The test method. *Journal of the Textile Institute*, *79*(3), 417–431. https://doi.org/10.1080/00405008808658276

Gassara, H. E., Barbier, G., Wagner Kocher, C., Sinoimeri, A., & Pumo, B. (2018). Experimental evaluation of transverse friction between fibers. *Tribology International*, *119* (October 2017), 112–122. https://doi.org/10.1016/j.triboint.2017.10.035

Goksoy, M. (1986). *A study of yarn-on-yarn abrasion*. PhD thesis, University of Manchester Institute of Science and Technology.

Hobbs, R. E., & Ridge, I. M. L. (2018). A new estimate of the yarn-on-yarn friction coefficient. *Journal of Strain Analysis for Engineering Design*, *53*(4), 191–196. https://doi.org/10.1177/0309324718760883

Leech, C. M. (2002). The modelling of friction in polymer fibre ropes. *International Journal of Mechanical Sciences*, *44*(3), 621–643. https://doi.org/10.1016/S0020-7403(01)00095-9

Lindberg, J., & Gralén, N. (1948). Measurement of Friction Between Single Fibers. *Swedish Institute for Textile Research, Gothenburg, Sweden*, 287–301.

Liu, L., Chen, J., & Zhu, B. (2006). The yarn-to-yarn friction of woven fabrics. *Proceeding of the 9th International ESAFORM Conference on Material Forming*, *November*, 4–7. http://www.wovencomposites.org/load03/esaform 2006 comp.pdf

Ridge, I. M. L., Banfield, S. J., & Mackay, J. (2010). Nylon fibre rope moorings for wave energy converters. *MTS/IEEE Seattle, OCEANS 2010*, *September*. https://doi.org/10.1109/OCEANS.2010.5663836

Tourlonias, M., Bueno, M. A., Fassi, G., Aktas, I., & Wielhorski, Y. (2019). Influence of friction angle between carbon single fibres and tows: Experimental analysis and analytical model. *Composites Part A: Applied Science and Manufacturing*, *124*(June). https://doi.org/10.1016/j.compositesa.2019.105478

Vu, T. D., Durville, D., & Davies, P. (2015). Finite element simulation of the mechanical behavior of synthetic braided ropes and validation on a tensile test. *International Journal of Solids and Structures*, *58*, 106–116. https://doi.org/10.1016/j.ijsolstr.2014.12.022

Weller, S. D., Johanning, L., Davies, P., & Banfield, S. J. (2015). Synthetic mooring ropes for marine renewable energy applications. *Renewable Energy*, *83*, 1268–1278. https://doi.org/10.1016/j.renene.2015.03.058